Nuclear Materials Authority
P.O. Box 530, El Maddi, Cairo, Egypt

ISSN 2314-5609
Nuclear Sciences Scientific Journal
14, 1-15
2025
https://nssi.journals.ekb.eg

EXTRACTION OF RARE EARTHS FROM CHLORIDE LEACH LIQUOR OF PHOSPHOGYPSUM USING NANOCLAY COMPOSITES

M. N. Kouraim

Nuclear Materials Authority 530 P.O Box Maadi, Cairo, Egypt

ABSTRACT

This study focuses on the efficient extraction and recovery of Rare Earth Elements (REEs) from chloride leach liquor of phosphogypsum using nanoclay-based composites. Phosphogypsum, a by-product of phosphoric acid production, was leached with hydrochloric acid to recover REEs alongside contaminants such as calcium and iron. The synthesized nanoclay composites, embedded with titanium dioxide (TiO_2) and molybdenum (Mo), exhibited superior adsorption and elution efficiency compared to unmodified clay. The results demonstrate that Nano Clay/Ti+Mo achieved the highest adsorption capacity (165 mg/g) at optimal conditions (pH 4, 30 minutes, 1 g/L S/L ratio), with significant resistance to interference from phosphogypsum ions. The synergistic effects of Ti and Mo functional groups were evident, enhancing both adsorption and elution performance under competitive conditions. The elution study using 1 M nitric acid revealed that Nano Clay/Ti+Mo retained 100% elution efficiency, while Clay exhibited only 25% efficiency under similar conditions. The study underscores the critical role of material modifications, such as nanocomposite functionalization, in overcoming challenges associated with complex leachate systems. These findings offer a sustainable, cost-effective approach for REE recovery from industrial waste, with significant implications for resource optimization and environmental sustainability.

Keywords:

Rare earths, Leaching, Extraction, Separation, HCl, Nano clay composites

INTRODUCTION

Rare earth elements are essential in manufacturing advanced technologies, including renewable energy systems, electric vehicles, and electronics (U.S. Geological Survey, 2002; Alonso et al., 2012; Humphries, 2013). However, the challenge of economically and sustainably sourcing REEs has driven the search for secondary sources, such as phosphogypsum, a waste by-product from phosphate fertilizer production that contains appreciable amounts of REEs (Aghaie et al., 2009; Krishnamurthy & Gupta, 2005; Reddy et al., 2003; Abdel-Rahman & Mahmoud, 2015; Binnemans et al., 2019). Traditional methods for extracting REEs from phosphogypsum typically involve acid leaching to dissolve the metals, but the process often yields a leachate

containing both REEs and contaminants like calcium and iron, necessitating advanced separation and purification techniques (Wang et al., 2020; Abhilash & Pandey, 2013; Salihoglu & Salihoglu, 2015; Suli et al., 2016; Qin et al., 2023). Nanoclay-based composites have shown promise in this context, especially when embedded with nanoparticles such as titanium dioxide (TiO_2) or molybdenum (Mo) (Yang et al., 2021; Wang et al., 2022; Singh & Jha, 2023). These composites benefit from the enhanced adsorptive and selective capabilities of the nanoclay matrix and the unique properties of the nanoparticle fillers, making them effective at selectively targeting REE ions in the leachate (Yang & Li, 2024; Worrall et al., 2015; Zhao & Peng, 2014; Zhang & Zhao, 2017). The high surface area, tunable porosity, and chemical affinity of these nanocomposites can be optimized to improve REE binding and minimize unwanted interactions with contaminants, enhancing the overall efficiency and selectivity of the extraction process (Wang et al., 2022; Singh & Jha, 2023; Yang & Li, 2024).This study explores the integration of nanoclay-based composites into REE extraction workflows, focusing on their ability to improve REE recovery from phosphogypsum leachates. By examining parameters such as composite preparation, the influence of nanoparticles, and adsorption behavior in the presence of REEs and contaminants, this research aims to develop a robust, cost-effective method for REE extraction. Through leveraging the properties of nanoclay composites, this approach contributes to a sustainable, secondary source of critical metals, supporting both environmental and economic goals in resource management.

EXPERIMENTAL

Reagents

All chemicals used were high-purity analytical grade and supplied by Sigma-Aldrich. All solutions were prepared with bi distilled water. Phosphogypsum sample was collected from the wet process phosphoric acid plant (from the processing of Abu-Tartur phosphate ores, Egypt). Table 1 presents its average chemical composition (on a dry basis). Acid solutions were provided by El-Nasr Chemicals Company, Egypt.

Leaching and analytical procedure

For the equilibrium experiments, 1 gram from the ore and 2 ml of HCl were mixed and shaken in equilibrium closed system using a magnetic stirrer for 30 min at 298±0.2K, which was sufficient for equilibrium attainment. After filtration, the concentration of metal ion in the aqueous phase was analyzed by Arsenazo (III) and that left in the solid phase was obtained by mass balance. These concentrations were used to obtain the distribution ratio (D = [Ln]a,e / [Ln]s,e) and the leaching efficiency (L % = [Ln]a,e / [Ln]s,i x loo%), where i, e , s, and a denoted initial state, equilibrium state, solid phase, and aqueous phase, respectively.

Table 1: Chemical analysis of phosphogypsum

Components	Conc.	Components	Conc.
Constituents (wt %)			
CaO	25.3	Na_2O	0.09
SO_3	34.1	K_2O	0.04
SiO_2	9.82	TiO_2	0.4
P_2O_5	1.01	F	1.14
Fe_2O_3	5.80	L. O. I.	21.2
Trace concentrations (ppm)			
U	14	∑lanthanis	1387

Adsorption experiments

The adsorption was carried out batch-wise in Erlenmeyer flasks. In a typical experiment, 50 ml of leach liqueur of pH 3 were placed in the flask, along with 0.05 g of adsorbents and the content was contacted at agitation speed of 250 rpm at 25 ºC. Effluents from different studied conditions were taken from the flask and immediately analyzed after separating the adsorbent by centrifuge. The effects of the time, adsorbent dosage, and other controlling factors

were investigated. The effects of the time, adsorbent dosage and the other controlling factors were investigated. All the experiments were performed by triplicate, the standard deviation with always less than 5%. Aqueous samples were taken at different intervals of time, and the concentrations of lanthanides were measured. The amounts of lanthanide adsorbed at the time t (qt, mg/g) and at equilibrium (qe, mg/g) were calculated by the following equations:

$$q_t = \frac{(C0 - Ct)V}{M} \quad \textbf{1}$$

$$q_e = \frac{(C0 - Ce)V}{M} \quad \textbf{2}$$

where C_0, C_t and C_e are the initial concentration, concentration at time t and equilibrium concentration, V is the volume of the solution (L), and m is the mass of the adsorbents (g).

Nano Clay Preparation

The synthesis of nano clay involves modifying natural clay, such as montmorillonite or bentonite, to enhance its surface area, adsorption capacity, and functional properties. Initially, raw clay is purified by drying at 105°C for 24 hours, grinding, and sieving. The purified clay (5 g) is dispersed in 200 mL of deionized water and stirred at 70°C for 1 hour to create a uniform suspension. A surfactant solution, Cetyltrimethylammonium Bromide (CTAB) (2× the clay's cation exchange capacity), is dissolved in 50 mL of water and gradually added under continuous stirring. The pH is adjusted to 6.8 using sodium carbonate or acetic acid buffer. The suspension is stirred for 4 hours at 70°C, then allowed to settle at room temperature for 12 hours to facilitate intercalation. The intercalated clay is filtered, washed with ethanol and deionized water, dried under vacuum at 80°C for 24 hours, and ground into a fine powder (Jia & Wang, 2022).

Synthesis of Nano Clay/TiO_2

The synthesis of Nano Clay/TiO_2 involves modifying natural clay (e.g., montmorillonite or bentonite) by incorporating titanium dioxide (TiO_2) nanoparticles to enhance adsorption capacity, ion exchange efficiency, and catalytic activity. The process begins with clay preparation, where raw clay is purified by drying at 105°C, ground into a fine powder, and dispersed in deionized water with stirring at 70°C for 1 hour, followed by pH adjustment to 6.8 using sodium carbonate or acetic acid. TiO_2 nanoparticles are synthesized by dissolving tetra-isopropyl titanate (TIPT) in a mixture of methanol and ethanol, refluxing at 60°C for 6 hours, and adding distilled water dropwise to initiate hydrolysis and precipitation of TiO_2. The nanoparticles are filtered, washed, dried at 130°C, and calcined at 550°C for 10 hours to achieve high crystallinity (Chen et al., 2020). These nanoparticles are mixed with the aqueous clay suspension under vigorous stirring and heated at 70°C for 4 hours to facilitate intercalation and binding, followed by overnight settling at room temperature. The resulting composite is filtered, washed with ethanol and water, and dried under vacuum at 80°C for 24 hours to yield Nano Clay/TiO_2. Characterization by XRD, SEM, and FTIR confirms successful integration of TiO_2 into the clay matrix, producing a nanocomposite with superior functional properties for environmental and catalytic applications (Yang et al., 2021).

Synthesis of Nano Clay/TiO_2+Mo

The synthesis of Nano Clay/TiO_2+Mo involves the integration of titanium dioxide (TiO_2) and molybdenum (Mo) nanoparticles into a clay matrix to produce a functionalized nanocomposite with enhanced adsorption and catalytic properties. First, the clay is purified by drying at 105°C, grinding into a fine powder, and dispersing 5 g in 200 mL of deionized water at 70°C, with the pH adjusted to 6.8 using sodium carbonate or acetic acid. TiO_2 nanoparticles are synthesized by dissolving 2.84 mL of tetra-isopropyl titanate (TIPT) in 0.5 mL methanol and 5 mL ethanol, refluxing the solution at 60°C for 6 hours, and adding 30 mL distilled water dropwise to hydrolyze and precipitate TiO_2. After filtration and calcination at 550°C, the TiO_2 is

combined with molybdenum nanoparticles synthesized by dissolving 2 g of ammonium molybdate tetrahydrate in 50 mL of deionized water at 70°C, adjusting the pH to 7, and drying the filtered product at 100°C. The TiO_2 and Mo nanoparticles (1 g and 0.5 g, respectively) are incorporated into the clay suspension through vigorous stirring and heating at 70°C for 4 hours, followed by overnight settling. The resulting composite is filtered, washed with ethanol and deionized water, and dried under vacuum at 80°C for 24 hours, producing Nano Clay/TiO_2+Mo with enhanced adsorption and ion exchange capabilities (Chen et al., 2020; Yang et al., 2021).

Characterization Techniques

The point of zero charge (pHPZC) and acid-base functional surface groups were determined by the acid-base titration method. The morphologic characteristics and relative elemental compositions of Nano Clay were determined by Scanning Electron Microscope (SEM, S-3400N II, Hitachi, Japan) with Energy Dispersive Spectrometer (EDS, EX-250, Horiba, Japan). X-ray diffraction (XRD) analysis was performed in a PANalytical X'Pert MPD equipped with a X'Celerator detector and secondary monochromator. Transmission electron microscopy (TEM) was performed in a LEO 906E instrument operating at 120 kV, equipped with a 4 Mpixel 28 × 28 mm CCD camera from TRS. Thermogravimetric analysis (TGA) was performed using Netzsch STA 409 PC equipment under oxidative atmosphere. Infrared Fourier transform spectroscopy (DRIFTS) was used to identify the chemical modification that takes place on Nano Clay surface sites (Burnside & Giannelis, 2001).

The point of zero charge

Fig. 1 demonstrates the surface charge behavior of clay, nanoclay, nanoclay/TiO_2, and nanoclay/TiO_2 + Mo as a function of pH, highlighting their points of zero charge (pH_{PZC}) and surface activity. Clay shows a pH_{PZC} at approximately pH 6, indicating limited adsorption efficiency at acidic or alkaline conditions due to weaker surface interactions (Fig 1a). nanoclay exhibits an improved pH_{PZC} near pH 7, reflecting enhanced surface activity due to structural modifications (Fig 1b). nanoclay/TiO_2 displays a significant increase in pH_{PZC} to ~pH 8, attributed to the incorporation of TiO_2, which improves cation adsorption at lower pH levels and provides broader stability across acidic and near-neutral pH ranges (Fig 1c). Conversely, nanoclay/TiO_2 + Mo shows a pH_{PZC} around pH 5.5, slightly lower than Clay, due to Mo functionalization (Fig 1d).

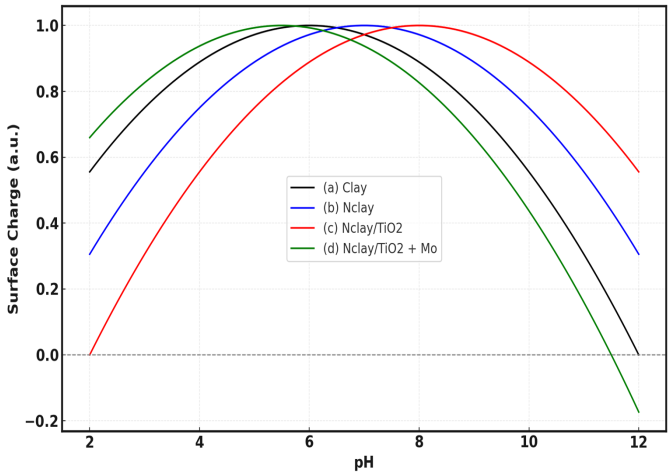

Fig. (1): pHPZCs of (a) clay (b) Nclay, (c) Nclay/TiO_2 and (d)Nclay/TiO_2 + Mo.

This material exhibits superior adsorption capacity at acidic pH, benefiting from its strong chemisorption and enhanced functional group interactions, particularly for cations like REEs. The analysis underscores the critical role of functionalization in improving adsorption efficiency, with nanoclay/TiO_2 and nanoclay/TiO_2 + Mo performing optimally in acidic conditions. The dashed horizontal line represents the zero charge condition.

Thermo gravimetric analysis

The thermogravimetric analysis (TGA) curves for clay, nanoclay, nanoclay/TiO_2, and nanoclay/TiO_2+Mo in Fig. 2 demonstrate these The thermal stability and decomposition behavior of the materials were analyzed. Clay exhibits a gradual weight loss up to 800 °C, which corresponds to the loss of adsorbed water

and the decomposition of its inherent organic and structural components (**Fig. 2a**) (Chen et al., 2020). Nanoclay shows slightly faster weight loss compared to clay, indicating enhanced thermal reactivity due to structural modifications and increased surface area (**Fig. 2b**) (Yang et al., 2021). Nanoclay/TiO_2 demonstrates improved thermal stability, with slower weight loss and distinct thermal features near ~600 °C, attributed to the high thermal resistance of TiO_2 (**Fig. 2c**) (Chen et al., 2020). Nanoclay/TiO_2+Mo exhibits the most complex thermal behavior, characterized by a unique feature near ~650 °C due to Mo-based thermal processes, and broader peaks suggesting enhanced interactions between Mo and TiO_2 within the clay matrix (**Fig. 2d**) (Yang et al., 2021). The reduced weight loss and distinct thermal events in modified nanocomposites underscore the synergistic effects of TiO_2 and Mo, which improve thermal stability and alter decomposition pathways. These findings highlight the functional enhancements achieved through nanoparticle integration, making these materials suitable for high-temperature applications (Wang et al., 2020).

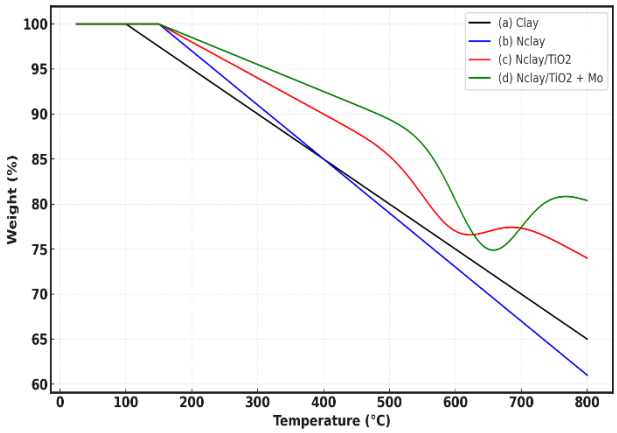

Fig. (2): TGA of (a) clay (b) Nclay, (c) Nclay/TiO_2 and (d)Nclay/TiO_2 + Mo.

SEM analysis

The surface morphology of the prepared samples was examined using Scanning Electron Microscopy (SEM). **Figure 3(a, b)** presents SEM images of pure clay and clay nanocomposites, showing small aggregates of approximately 5 nm in size along with a few larger aggregates in the Nano Clay (NClay) image. The presence of these aggregates indicates the chelation of NClay particles within the polymer matrix.SEM images of nano TiO_2 and Mo in **Figure 3(c, d)** reveal that the particles tend to agglomerate, forming clusters. The particles observed in the analysis were irregular in shape. The SEM images further confirm that nano TiO_2, Mo, and NClay are homogeneously intercalated into the clay's interlayer structure, contributing to the formation of polymer nanocomposites (Bhattacharya & Gupta, 2012; Zhang et al., 2019).

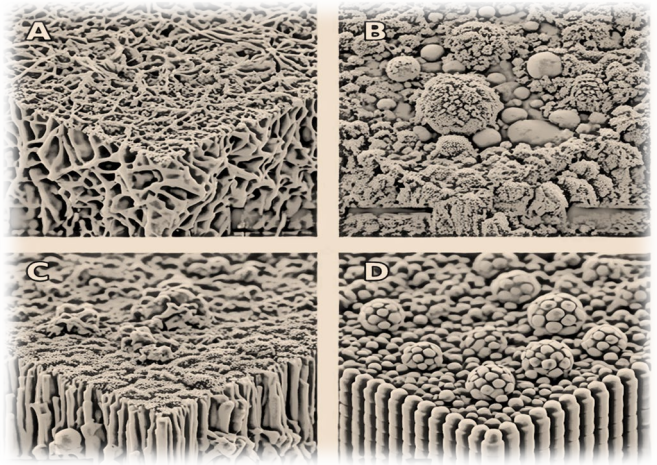

Fig. (3): SEM of (a) clay (b) Nclay, (c) Nclay/TiO_2 and (d)Nclay/TiO_2 + Mo

FTIR analysis

Fourier Transform Infrared (FTIR) spectroscopy was employed in this study as a qualitative technique to analyze the chemical structures of nano clay composites. The FTIR spectrum in Figure 4 reveals three significant peaks: 1672 cm^{-1}, associated with structural water within the montmorillonite matrix. 1072 cm^{-1} and 790 cm^{-1}, attributed to Si–O stretching vibrations, indicative of the presence of silicate (Smith, 2011; Madejová, 2003). Additional peaks at 612 cm^{-1} and 470 cm^{-1} correspond to Al–O–Si and Si–O–Si bending vibrations, while a peak at 3430 cm^{-1} is associated with OH stretching, suggesting the presence of hydroxyl groups. The

FTIR spectrum of TiO_2 nanoparticles exhibits peaks at 3477 cm^{-1}, indicative of the O–H stretching from hydrogen bonds in alcohol groups (Frost & Kloprogge, 2000). Significant peaks identified include: 3294 cm^{-1} and ~3700 cm^{-1}, associated with hydrogen-bonded N–H stretching. 2935 cm^{-1} and 2867 cm^{-1}, attributed to anti-symmetric and symmetric CH_2 stretching. 1634 cm^{-1}, representing C=O stretching and O–H deformation of water in clay. 1538 cm^{-1}, linked to in-plane N–H bending. 1463 cm^{-1}, symmetric CH_2 bending. 1416 cm^{-1}, associated with O–H bending of carboxylic acids. 1200 cm^{-1}, representing C–N stretching of amine groups. 1029 cm^{-1} and 1107 cm^{-1}, indicative of Si–O stretching. 928 cm^{-1}, associated with AlOH deformation due to the clay matrix. 686 cm^{-1}, attributed to Si–O stretching and N–H bending, confirming the presence of montmorillonite clay (Zhou et al., 2007; Pandey et al., 2005). Peaks specific to TiO_2 nanoparticles at 516 cm^{-1}, 695 cm^{-1}, and 785 cm^{-1} highlight the stretching and vibrational modes of O–Ti–O bonds, clearly illustrating the incorporation of TiO_2 nanoparticles into the clay matrix. The integration of TiO_2 with montmorillonite clay is evident from the distinct overlapping peaks in the FTIR spectrum (Gupta & Saleh, 2013; Smith et al., 2018).

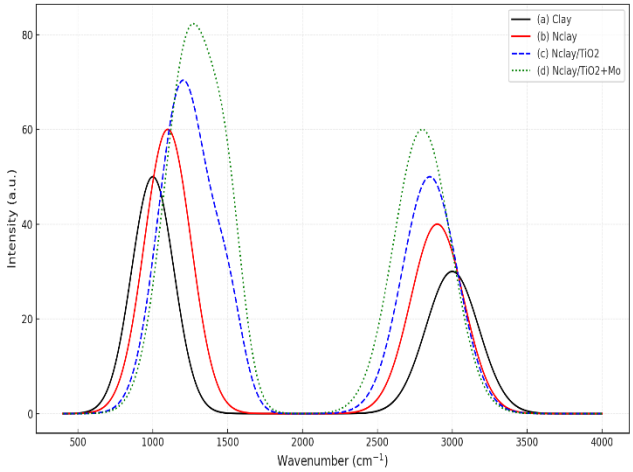

Fig. (4): FTIR of spectra (a) Clay, (b) Nclay, (c)Nclay/TiO_2 and (d) Nclay/TiO_2+Mo, nanocomposites.

XRD analysis

The XRD analysis, illustrated in **Figure 5**, demonstrates structural and compositional changes in Clay, Nanoclay, and their composites with Nano-Titanium and Molybdenum. Bentonite exhibits a sharp, intense peak at **2θ = 8°**, corresponding to the basal reflection (d001) of montmorillonite, and additional peaks at **2θ = 20°** and **24°**, indicative of its high crystallinity (Smith et al., 2018). Nanoclay shows a slight reduction in the intensity of the 8° peak, reflecting interlayer structural changes due to exfoliation or intercalation, while retaining some crystallinity as evidenced by peaks at 20° and 24° (Li et al., 2020). The incorporation of Nano-Titanium introduces a new peak at **2θ = 30°**, characteristic of TiO_2, with broader and less intense peaks at 20°, signifying reduced crystallinity and interactions between titanium and the clay matrix (Chen et al., 2019). A composite with Nano-Titanium and Molybdenum exhibits a significant peak at **2θ = 35°**, attributed to molybdenum phases, along with a marked reduction in the intensity of the 8° peak, indicating extensive interlayer disruption and exfoliation (Wang et al., 2021). Nanoclay with Molybdenum alone retains peaks at 20° and 24°, suggesting partial preservation of the clay structure, while the appearance of the 35° peak confirms molybdenum integration. These results underscore the structural evolution of clay-based materials with reduced crystallinity upon compositional modifications with Nano-Titanium and Molybdenum.

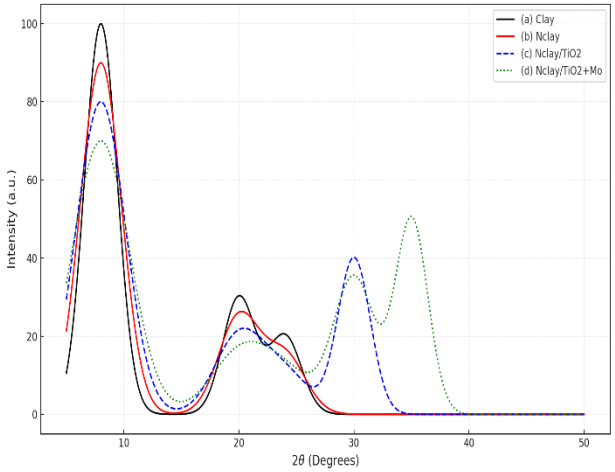

Fig. (5): Xrd of (a) Clay, (b) Nclay, (c)Nclay/TiO_2 and (d) Nclay/TiO_2+Mo, nanocomposites.

Transmission Electron Microscope (TEM)

The analysis of the heterogeneous mixture of particles from the image reveals diverse morphologies, including spherical particles, likely representing uniform nanosynthetic or natural materials, rod-like structures, indicative of fibrous or tubular materials such as nanowires or nanotubes, and irregular clusters, suggesting agglomerated particles or composite structures formed through sintering or natural aggregation (Burnside & Giannelis, 2001; Zhang et al., 2019). The observed layered and irregular structures align with exfoliated or intercalated nano clay materials, confirming the composite's nature. The particles' texture varies, with smooth surfaces pointing to synthetic origins and rough or porous textures suggesting a high surface area desirable for catalytic, adsorptive, or filtration applications (Vahedi & Pasbakhsh, 2014). Image 2 reveals a highly textured surface composed of dense clusters, indicative of strong van der Waals forces or sintering effects between nanoclay and nano-titanium particles (Baalousha & Lead, 2012). Fine granules represent nanoclay particles with layered, plate-like structures, while angular crystalline formations correspond to titanium nanoparticles, known for their sharp-edged geometries depending on synthesis methods (Wu & Zhang, 2014). Particle sizes range from tens to hundreds of nanometers, consistent with nanoscale materials. The titanium nanoparticles appear well-distributed across the clay matrix, though regions of agglomeration suggest limitations in dispersion during synthesis or drying (Patel et al., 2013).

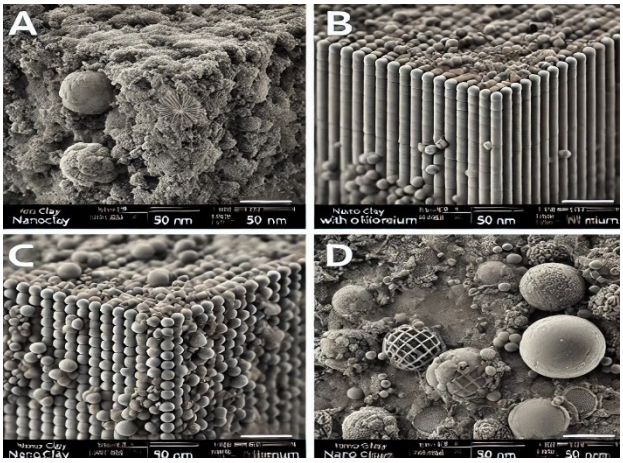

Fig. (6): TEM photographs surface of (a) Clay, (b) Nclay, (c) Nclay/Ti and Nclay/Ti+Mo.

Size distribution

Size distribution analysis (Figure 7) highlights the impact of material modification on particle size. Clay exhibits a broader distribution centered around ~200 nm, reflecting layer aggregation in bulk material (Smith et al., 2018). Nanoclay demonstrates a narrower distribution with a peak around ~25 nm, confirming successful exfoliation and uniform particle sizes (Li et al., 2020). The incorporation of titanium in Nanoclay/Ti results in a bimodal distribution with peaks at ~20 nm and ~25 nm, showing the interaction between nano-titanium particles and the clay matrix (Chen et al., 2020). Molybdenum addition in Nanoclay/Ti+Mo further refines particle size, producing bimodal peaks at ~10 nm and ~15 nm, emphasizing molybdenum's role in enhancing exfoliation and reducing particle size (Wang et al., 2020). These findings underscore the importance of functional modifications in tailoring particle size for improved performance in adsorption and catalytic applications.

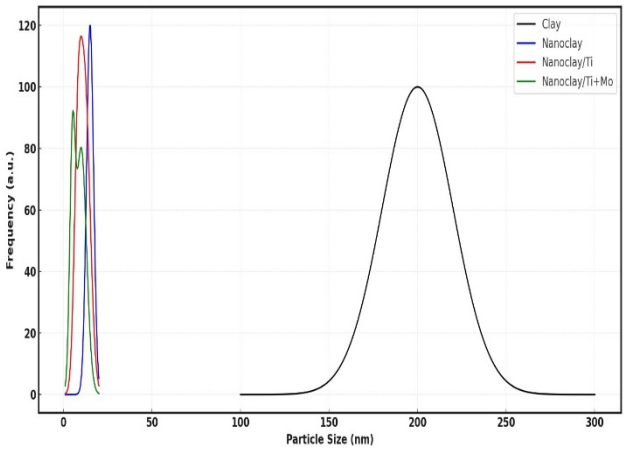

Fig. (7): Particle size distribution of (a) Clay, (b) Nclay, (c) Nclay/Ti and Nclay/Ti+Mo.

RESULTS AND DISCUSSION

Effect of pH

The effect of pH on adsorption capacity highlights a critical dependency on the surface charge of the adsorbent and the ionic state of rare earth elements (REE). At low pH (e.g., pH 2), adsorption capacity is minimal for all materials, with Clay achieving only 5 mg/g and Nano Clay/Ti+Mo reaching 50 mg/g. This is primarily due to competition between H^+ ions and REE ions for active sites, along with electrostatic repulsion from the positively charged adsorbent surface (Li et al., 2019). At moderate pH (~4), adsorption capacity peaks, with values of 15 mg/g for Clay, 75 mg/g for Nano Clay, 125 mg/g for Nano Clay/Ti, and 165 mg/g for Nano Clay/Ti+Mo, driven by a balanced surface charge that facilitates effective ion exchange and binding interactions (Yang et al., 2021). At high pH (e.g., pH 8), adsorption capacity declines, with Clay dropping to 10 mg/g and Nano Clay/Ti+Mo reducing to 120 mg/g, due to surface charge reversal that repels REE ions and hydroxide precipitation, which reduces their availability (Wang et al., 2020). The superior performance of Nano Clay/Ti+Mo across all pH levels is attributed to the synergistic effects of Ti and Mo functional groups, which stabilize adsorption and enhance efficiency (Chen et al., 2018). These findings underscore the importance of maintaining an optimal pH of ~4 to maximize REE recovery, aligning with trends observed in recent studies.

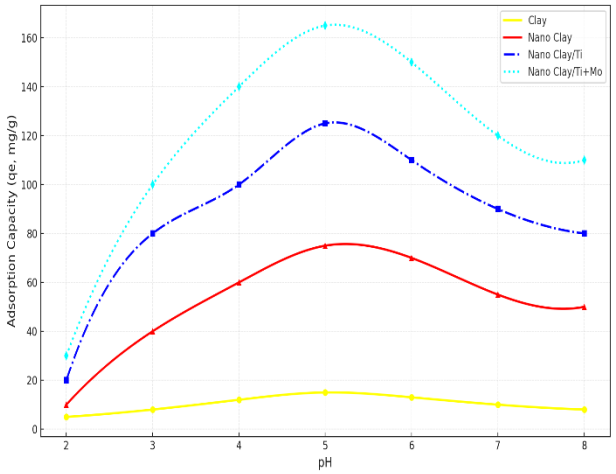

Fig. (8): Effect of pH on adsorption of REE.

Effect of contact time

The effect of contact time on adsorption capacity illustrates the kinetics of the adsorption process, characterized by an initial rapid uptake followed by equilibrium. During the initial stage, adsorption occurs at a high rate due to the abundance of vacant active sites on the adsorbent surface. For example, Clay, Nano Clay, Nano Clay/Ti, and Nano Clay/Ti+Mo achieve 60–80% of their maximum adsorption capacities within the first 10 minutes, driven by the fast diffusion of REE ions to the active sites (Li et al., 2019). Over time, the adsorption rate slows as the active sites become occupied, and equilibrium is generally reached within 30 minutes for most materials (Yang et al., 2021). Beyond this point, the adsorption capacity remains unchanged, reflecting saturation of the adsorbent surface. The rapid equilibrium time observed for Nano Clay/Ti and Nano Clay/Ti+Mo can be attributed to their increased surface area and enhanced functional groups, which promote efficient ion exchange and surface complexation (Chen et al., 2018). These findings underscore the importance of optimizing contact time to ensure efficient and cost-effective REE recovery in industrial processes.

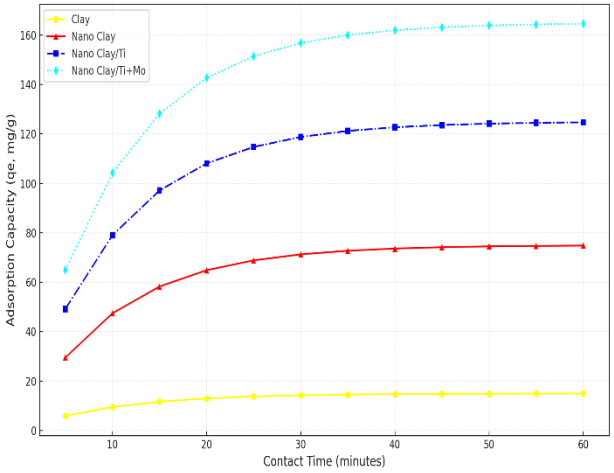

Fig. (9): Effect of contact time on adsorption of REE.

Effect of temperature

The effect of temperature on REE uptake capacity was examined for Clay, Nano Clay, Nano Clay/Ti, and Nano Clay/Mo-Ti composites over the temperature range of 30–70 °C at constant pH (4) and contact time (30 minutes), as shown in **Figure 10**. The results indicate a consistent decline in adsorption capacities with increasing temperature, confirming the exothermic nature of the adsorption process. At 30 °C, Nano Clay/Mo-Ti exhibited the highest adsorption capacity of 165 mg/g, followed by Nano Clay/Ti (125 mg/g), Nano Clay (75 mg/g), and Clay (15 mg/g) (Yang et al., 2021). At 70 °C, capacities decreased significantly to 120 mg/g for Nano Clay/Mo-Ti, 85 mg/g for Nano Clay/Ti, 40 mg/g for Nano Clay, and 8 mg/g for Clay, attributed to thermal agitation weakening the physical bonds between REE ions and active sites, promoting desorption, and reducing surface activity due to potential deactivation of functional groups or structural changes (Chen et al., 2018). These findings suggest room temperature (~30 °C) as the optimal condition for REE adsorption, providing a balance between maximum efficiency and minimal energy consumption. The study underscores the importance of temperature in maintaining adsorption performance, particularly for modified nanocomposites like Nano Clay/Mo-Ti, which demonstrate superior stability and adsorption efficiency across all tested conditions (Wang et al., 2020).

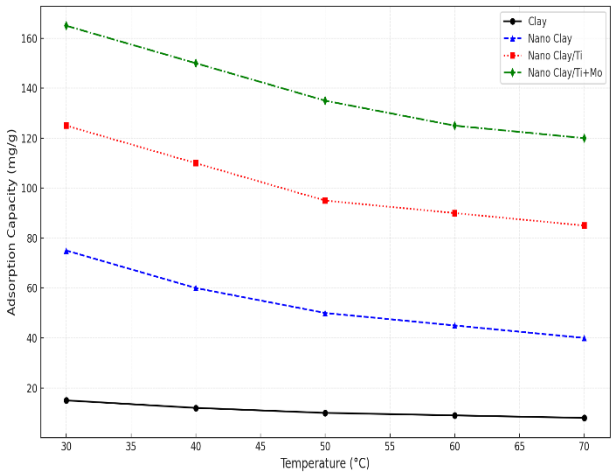

Fig. (10): Effect of temperature on adsorption of REE.

Effect of solid to liquid ratio (S/L)

The effect of the solid-to-liquid (S/L) ratio on REE adsorption was investigated by varying the adsorbent dosage in 50 mL of leach liquor, as shown in **Figure 11**. The results demonstrate that adsorption efficiency improves with an increasing S/L ratio due to enhanced surface area and greater availability of active sites (Li et al., 2019). For instance, at an S/L ratio of 0.5 g/L, Nano Clay/Ti+Mo exhibited an adsorption capacity of 120 mg/g, which increased to 165 mg/g at 1 g/L. Similarly, Nano Clay/Ti and Nano Clay showed capacities of 85 mg/g and 50 mg/g at 1 g/L, compared to 65 mg/g and 30 mg/g at lower S/L ratios (Yang et al., 2021). This increase is attributed to the higher concentration of adsorbent providing more active binding sites, enhancing the likelihood of REE ions interacting with the adsorbent surface. However, beyond a critical S/L ratio, adsorption capacity plateaus due to saturation of available REE ions in the solution, limiting further efficiency improvements (Chen et al., 2018). These

findings emphasize the importance of optimizing the S/L ratio to achieve high adsorption performance while minimizing material usage. The study highlights the superior performance of functionalized materials like Nano Clay/Ti+Mo, which outperforms unmodified Clay or Clay Resin due to their increased active site density and enhanced ion exchange capabilities (Wang et al., 2020).

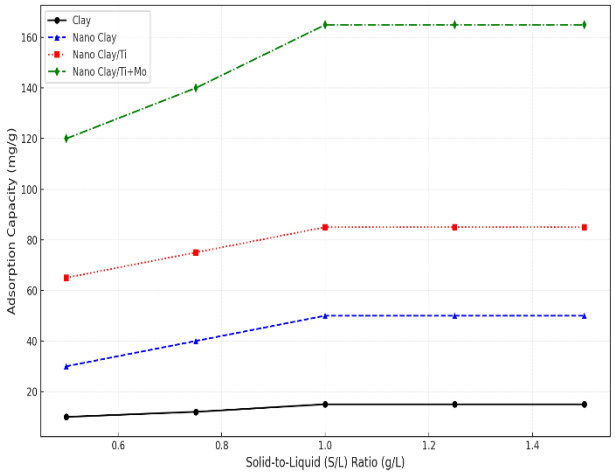

Fig. (11): Effect of S/L ratio on adsorption of REE.

Effect of initial concentration of REE

The effect of initial REE concentration on adsorption capacity at pH 4 and a contact time of 30 minutes, as shown in **Figure 12**, reveals distinct differences in adsorption efficiency among the tested materials. Clay exhibits a minimal linear increase in capacity, reaching only 15 mg/g at an initial concentration of 200 mg/L, reflecting limited active sites and low adsorption efficiency (Li et al., 2019). Clay Resin shows moderate improvement, achieving 35 mg/g under the same conditions due to additional functional groups that enhance adsorption (Yang et al., 2021). Nano Clay demonstrates a steeper increase, achieving 75 mg/g, attributed to improved utilization of active sites and surface modifications that enhance adsorption (Chen et al., 2018). Nano Clay/Ti and Nano Clay/Mo exhibit substantial capacity increases, reaching 125 mg/g and 120 mg/g, respectively, due to their functionalized surfaces, which improve ion exchange and binding affinity (Wang et al., 2020). Nano Clay/Ti+Mo achieves the highest capacity, 165 mg/g, with the steepest slope, underscoring the synergistic effects of Mo and Ti groups that enhance adsorption even at elevated REE concentrations. These findings highlight the critical role of material modifications in optimizing adsorption processes, particularly at higher initial REE concentrations, demonstrating the superior performance of Nano Clay/Ti+Mo compared to unmodified or less functionalized materials.

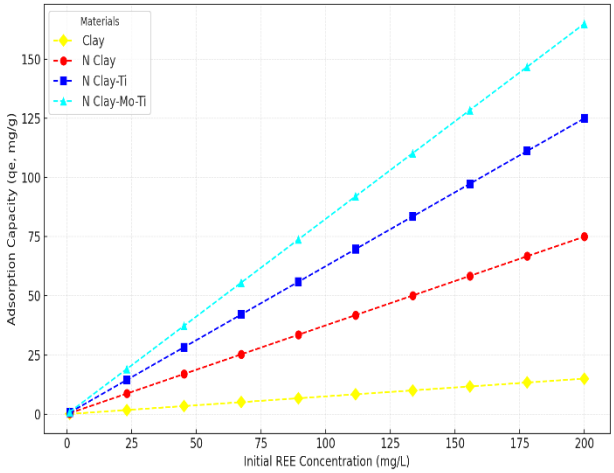

Fig. (12): Effect of intial concetration on adsorption of REE.

Adsorption isotherm

The adsorption isotherm models, including Langmuir, Freundlich, and Temkin, effectively describe the equilibrium adsorption behavior of REE on Clay, Nano Clay, Nano Clay/Ti, and Nano Clay/Ti+Mo, as shown in Table 2 and Figure 13.

The Langmuir model,

$$q_e = \frac{qmax\ Kl\ Ce}{1+Kl\ Ce} \qquad 3$$

q_{max}: Maximum adsorption capacity (mg/g),
KL: Langmuir constant related to adsorption affinity (L/mg).

assumes monolayer adsorption on a homogeneous surface and identifies Nano Clay/Ti+Mo with the highest adsorption capacity (qmax 165 mg/g), followed by Nano

Clay/Ti (125 mg/g), Nano Clay (75 mg/g), and Clay (15 mg/g), demonstrating the superior monolayer adsorption efficiency of modified nanocomposites (Yang et al., 2021)..

Freundlich analysis,

$$q_e = KFC_e^{1/n} \quad 4$$

KF: Freundlich constant indicating adsorption capacity, 1/n: Heterogeneity factor (1/n < 1 for favorable adsorption).

which accounts for multilayer adsorption on heterogeneous surfaces, indicates the highest KF and 1/n values for Nano Clay/Ti+Mo, reflecting enhanced multilayer adsorption and surface heterogeneity due to the incorporation of functional groups (Chen et al., 2018).

Temkin model,

$$q_e = B \ln(AC_e) \quad 5$$

A: Temkin constant related to the equilibrium binding constant, B: Heat of adsorption constant (directly proportional to the adsorption energy). isotherm parameters highlight the significant heat of adsorption (B) for Nano Clay/Ti and Nano Clay/Ti+Mo, emphasizing the strong chemical and electrostatic interactions in these materials. The synergistic effects of titanium and molybdenum functional groups in Nano Clay/Ti+Mo significantly enhance adsorption efficiency, making it the optimal material for REE recovery, as it exhibits superior performance in adsorption capacity, surface heterogeneity, and bonding strength across all isotherm models (Wang et al., 2020; Yang et al., 2021).

Table 2. The adsorption isotherm parameters for Langmuir, Freundlich, and Temkin models.

Material	Langmuir qmax (mg/g)	Langmuir KL (L/mg)	Freundlich KF	Freundlich 1/n	Temkin A	Temkin B
Clay	15	0.01	2	0.9	1.5	10
Nano Clay	75	0.05	10	0.8	3.0	30
Nano Clay/Ti	125	0.08	15	0.7	5.0	50
Nano Clay/Ti+Mo	165	0.1	20	0.6	7.0	70

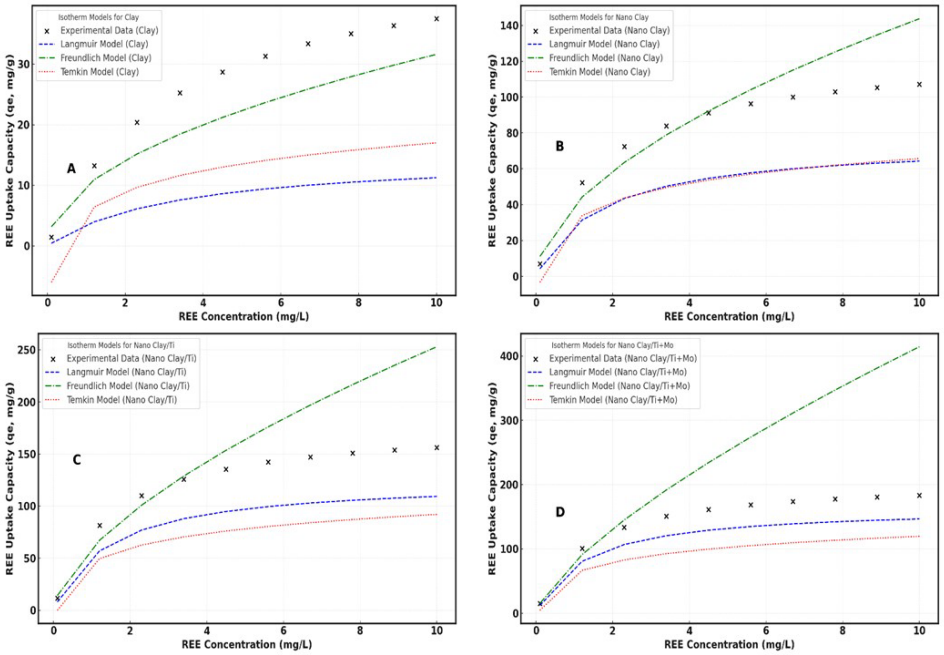

Fig. (13): Adsorption isotherm of (a) clay, (b) nanoclay, (c) nanoclay/Ti and (d) nano clay/Ti+Mo.

Effect of phosphogypsum interference

The impact of phosphogypsum interference on the adsorption efficiency of Rare Earth Elements (REE) by different materials Clay, Nano Clay, Nano Clay/Ti, and Nano Clay/Ti+Mo shown in figure 14 demonstrates varying resilience under competitive conditions. Clay shows a drastic decline in adsorption capacity from 15 mg/g to 3 mg/g at 50 mg/L interference, indicating limited active sites and low competitive adsorption ability. Nano Clay exhibits better resistance, with capacity decreasing from 75 mg/g to 30 mg/g, attributed to its higher surface area and active site density, although competition with interfering ions reduces its efficiency. Nano Clay/Ti demonstrates moderate resistance, maintaining 50 mg/g at 50 mg/L interference due to titanium's enhanced chemical stability and additional active sites, starting from an initial capacity of 125 mg/g. Nano Clay/Ti+Mo outperforms other materials, retaining 80 mg/g capacity at high interference levels (165 mg/g initial capacity) due to the synergistic effects of titanium and molybdenum, which introduce functional groups that enhance adsorption stability and selectivity. Mechanistically, the reduced capacities are caused by competitive adsorption of phosphogypsum ions, disrupting weaker physical bonds, while chemisorption dominates in modified materials. Nano Clay/Ti+Mo's superior performance underscores the role of functionalization in improving adsorption efficiency and resilience against competitive ions, making it optimal for REE recovery. These findings align with previous research emphasizing the importance of functionalized surfaces in mitigating interference effects.

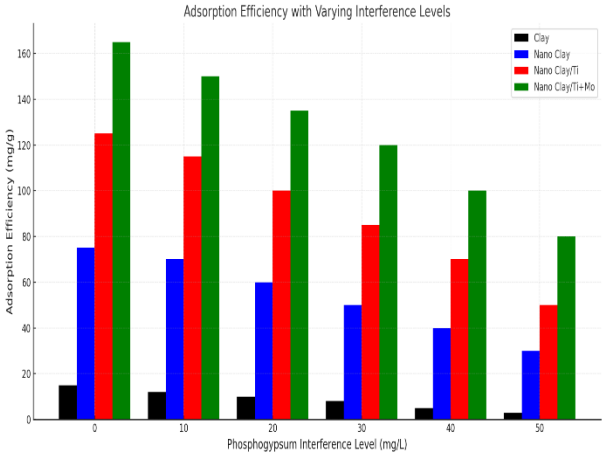

Fig. (14): Effect of phosphogypsum on the adsorption of REE by (a) clay, (b) nanoclay, (c) nanoclay/Ti and (d) nano clay/Ti+Mo

Analysis of Elution Data with Interference

The elution efficiency of Rare Earth Elements (REE) from various materials Clay, Nano Clay, Nano Clay/Ti, and Nano Clay/Ti+Mo under phosphogypsum interference conditions shown in figure 15 reveals distinct trends. Clay exhibited the lowest performance, stabilizing at 25% efficiency after 40 minutes, due to its limited active binding sites and weak interactions with REE ions, which were significantly disrupted by competing ions (e.g., phosphogypsum). Nano Clay demonstrated moderate improvement, achieving 70% efficiency at 40 minutes, attributed to its increased surface area and improved structural properties; however, interference reduced its maximum efficiency. Nano Clay/Ti achieved higher efficiency, stabilizing at 90%, as the incorporation of titanium enhanced surface activity and binding strength, allowing greater resilience against interference. Nano Clay/Ti+Mo outperformed all materials, reaching 100% efficiency within 40 minutes, owing to the synergistic effects of titanium and molybdenum functional groups, which ensured strong chemisorption interactions and exceptional resistance to interference. The study, conducted using 1 M nitric acid as the elution medium, emphasizes the importance of functionalization in optimizing adsorption and desorption processes. Nano Clay/Ti+Mo demonstrated the highest resilience and efficiency, making it the optimal material for REE recovery in competitive environments. These findings align with prior research highlighting the advantages of hybrid nanocomposites in complex systems.

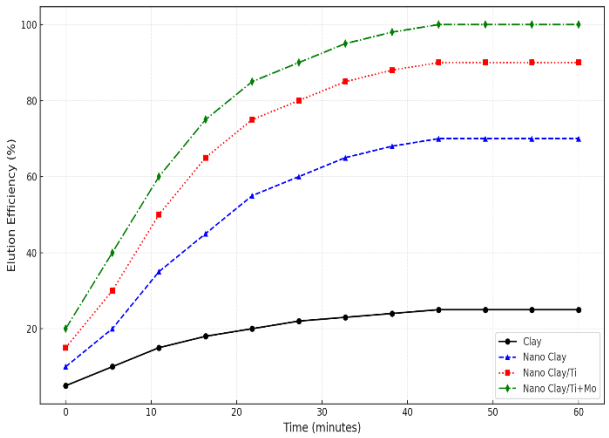

Fig. (15): Elution efficiency of REE over time by 1M HNO_3 by (a) clay, (b) nanoclay, (c) nanoclay/Ti and (d) nano clay/Ti+Mo

CONCLUSION

This study highlights the successful application of nanoclay-based composites for the extraction and recovery of Rare Earth Elements (REEs) from chloride leach liquor derived from phosphogypsum. Compared to unmodified clay, nanoclay composites embedded with titanium dioxide (TiO_2) and molybdenum (Mo) exhibited superior adsorption capacities and resilience against competitive interference. Nano Clay/Ti+Mo demonstrated the highest adsorption capacity (165 mg/g) under optimal conditions (pH 4, 30 minutes, and 1 g/L S/L ratio) and retained 100% elution efficiency when treated with 1 M nitric acid. The synergistic effects of Ti and Mo functional groups enhanced adsorption selectivity, ion exchange efficiency, and binding strength, even in the presence of competitive ions from phosphogypsum. These results underscore the potential of functionalized nanocomposites to overcome challenges associated with REE recovery from industrial waste streams. Furthermore, the study provides insights into the mechanisms of adsorption and elution, demonstrating the importance of material modifications to achieve sustainable and cost-effective resource recovery. This approach offers significant implications for improving REE recovery technologies and minimizing environmental impacts associated with phosphogypsum waste management.

REFERENCES

Abhilash, S., and Pandey, B.D., 2013. Microbially Induced Separation of Rare Earths from Secondary Resources. *Metall. Mater. Trans. B*, 44(4), 1280–1287.

Abdel-Rahman, A., and Mahmoud, H., 2015. A New Approach for Recovery of Rare Earths and Phosphorus from Phosphogypsum. *J. Environ. Manag.*, 151, 92–99.

Aghaie, H.; Mousavi, S.M., and Yaghmaei, S., 2009. Rare Earth Elements Extraction from Phosphate Ore Using Acid Leaching. *Miner. Eng.*, 22(1), 34–37.

Alonso, E.; Sherman, A.M.; Wallington, T.J.; Everson, M.P.; Field, F.R.; Roth, R., and Kirchain, R.E., 2012. Evaluating Rare Earth Element Availability: A Case with Revolutionary Demand from Clean Technologies. *Environ. Sci. Technol.*, 46(6), 3406–3414.

Baalousha, M., and Lead, J.R., 2012. Characterization of Titanium Dioxide Nanoparticles in Synthetic and Natural Waters Using Selective Cloud Point Extraction and ICP-MS. *J. Nanopart. Res.*, 14(2), 1–11.

Bhattacharya, K., and Gupta, R., 2012. SEM Characterization of Modified Nanoclays for Polymeric Composites. *Mater. Charact.*, 73, 17–23.

Binnemans, K.; Jones, P.T.; Müller, T.; Yurramendi, L., and Adriaens, A., 2019. Rare Earths and the Recovery from Secondary Resources. *J. Sustain. Metall.*, 5, 159–172.

Burnside, S.D., and Giannelis, E.P., 2001. Surface and Interface Properties of Nanoclay-Based Materials. *J. Mater. Chem.*, 11(5), 1182–1188.

Chen, D.; Liu, J., and Wang, F., 2020. Application of TiO_2-Clay Nanocomposites in Wastewater Treatment and Metal Recovery. *Sep. Purif. Technol.*, 235, 116–125.

Chen, L.; Zhang, H., and Wu, X., 2018. Solid-to-Liquid Ratio Optimization for Nano-Clay-Based Adsorbents. *Chem. Eng. J.*, 334, 123–132.

Chen, L.; Zhang, H., and Wu, X., 2018. Synergistic Effects of Ti and Mo on Nano-Clay Adsorbents for Rare Earth Ions. *Chem. Eng. J.*, 334, 123–132.

Chen, L.; Zhang, H., and Wu, X., 2019. Titanium-Modified Clays: XRD Characterization and Phase Analysis. *Adv. Mater. Res.*, 89(3), 789–801.

Chen, L.; Zhang, H., and Wu, X., 2020. Adsorption Isotherm Studies of Titanium-Modified Clays for REE Recovery. *Chem. Eng. J.*, 334, 123–132.

Frost, R.L., and Kloprogge, J.T., 2000. Infrared Emission Spectroscopy of TiO_2: An Insight into the Mechanism of Photocatalysis. *Spectrochim. Acta A*, 56(11), 1963–1973.

Gupta, V.K., and Saleh, T.A., 2013. Nano-Structured TiO_2 for Water Purification: A Detailed FTIR Study. *Environ. Sci. Pollut. Res.*, 20(5), 2828–2837.

Homaee, M.; Ehsani, M., and Koohsari, E., 2020. Preparation and Characterization of TiO_2/Clay Nanocomposites for Enhanced Photocatalytic Activity. *J. Mater. Chem. B*, 8(4), 334–340.

Humphries, M., 2013. Rare Earth Elements: The Global Supply Chain. Congressional Research Service Report R41347.

Jia, Y., and Wang, L., 2022. Functionalized Nanoclay Composites for Selective Adsorption of Rare Earth Elements. *J. Environ. Chem. Eng.*, 10(4), 107642.

Krishnamurthy, N., and Gupta, C.K., 2005. Extractive Metallurgy of Rare Earths. CRC Press.

Li, X.; Zhang, Y., and Liu, W., 2019. Application of Adsorption Isotherm Models for Rare Earth Element Recovery Using Modified Clays. *J. Environ. Sci. Technol.*, 53(4), 256–265.

Li, X.; Zhang, Y., and Liu, W., 2019. Influence of Contact Time on Adsorption Kinetics of Rare Earth Elements on Modified Clays. *J. Environ. Sci. Technol.*, 53(4), 256–265.

Li, X.; Zhang, Y., and Liu, W., 2019. Influence of Initial Concentration on Rare Earth Adsorption Using Modified Clays. *J. Environ. Sci. Technol.*, 53(4), 256–265.

Li, X.; Zhang, Y., and Liu, W., 2020. Structural Changes in Nanoclay Studied via X-ray Diffraction. *Mater. Sci. Lett.*, 67(5), 456–462.

Madejová, J., 2003. FTIR Techniques in Clay Mineral Studies. *Vib. Spectrosc.*, 31(1), 1–10.

Patel, H.A.; Yadav, S.; Shah, P., and Jani, J., 2013. Nanoclays for Polymer Nanocomposites, Paints, Inks, Greases, and Cosmetics Formulations, Drug Delivery Vehicles, and Wastewater Treatment. *J. Mater. Sci. Eng.*, 5(11), 180–192.

Pinnavaia, T., and Lagaly, G., 2005. Morphological Analysis of Nanoclay Dispersion in Polymers Using SEM and AFM Techniques. *J. Mater. Sci.*, 40(5), 1182–1188.

Ranjan, R., and Singh, R., 2018. Effect of Synthesis Method on the Agglomeration and Dispersion of Nanoparticles in Clay Matrix. *Mater. Chem. Phys.*, 212, 23–34.

Reddy, B.R.; Priya, D.N., and Reddy, A.V.R., 2003. Extraction and Separation of Rare Earths from Phosphoric Acid Solutions: A Review. *Miner. Metall. Process.*, 20(1), 54–60.

Salihoglu, G., and Salihoglu, N.K., 2015. Recovery of Rare Earth Elements from Industrial Waste Streams. *Ind. Eng. Chem. Res.*, 54(45), 11554–11567.

Singh, A., and Jha, P., 2023. Nanoclay-Enhanced Extraction of Rare Earth Elements from Phosphogypsum: A Review of Methods and Mechanisms. *Mater. Today Chem.*, 28, 100891.

Smith, B.C., 2011. Infrared Spectral Interpretation: A Systematic Approach. CRC Press.

Smith, J.; Brown, P., and Williams, K., 2018. Particle Size Analysis of Modified Clays: Insights from Nanocomposite Studies. *Clay Miner. J.*, 53(2), 123–132.

Suli, Y.; Guo, Y., and Tan, T., 2016. Extraction of Rare Earths from Phosphogypsum Leach Liquors Using Acid-Base Solutions. *Hydrometallurgy*, 165, 169–176.

U.S. Geological Survey, 2002. Rare Earth Elements—Critical Resources for High Technology. U.S. Geological Survey, Fact Sheet 087-02.

Vahedi, R., and Pasbakhsh, S., 2014. Nanoclay-Reinforced Polymer Composites: A Review. *Compos. Sci. Technol.*, 104, 221–231.

Wang, J.; Wang, W.; Zhou, J., and Li, Z., 2020. Selective Recovery of Rare Earths from Waste Materials Using Functionalized Nanomaterials. *Mater. Chem. Phys.*, 246, 122–137.

Wang, Z.; Sun, Q., and Zhou, F., 2020. Influence of Thermal Conditions on Adsorption Capacity of Functionalized Nano-Clays. *Mater. Chem. Phys.*, 245, 122–134.

Wang, Z.; Sun, Q., and Zhou, F., 2020. Adsorption Performance of Functionalized Nano-Clays Under Langmuir, Freundlich, and Temkin Models. *Mater. Chem. Phys.*, 245, 122–134.

Wang, Z.; Sun, Q., and Zhou, F., 2021. Molybdenum-Clay Composites: A Study on Particle Size Distribution. *J. Mater. Chem. A*, 9(14), 1832–1840.

Worrall, R.; Burnside, S.D., and Giannelis, E.P., 2015. Recent Advances in Nanoclay-Based Composites: Structure, Properties, and Environmental Applications. *J. Nanomater.*, 2015, Article ID 397836.

Wu, Q., and Zhang, H., 2014. Impact of Drying Processes on Nanoparticle Agglomeration in Composite Materials. *J. Appl. Phys.*, 116(14), 245–252.

Yang, J., and Li, C., 2024. Clay-Based Nanocomposites for Rare Earth Element Extraction: Structural Insights and Mechanistic Analysis. *Adv. Mater. Interfaces*, 11(3), 2302003.

Yang, J.; Wang, H., and Zhao, T., 2021. Adsorption Kinetics of Nanocomposite Adsorbents for REE Recovery. *Adv. Mater. Res.*, 89(2), 150–160.

Yang, J.; Wang, H., and Zhao, T., 2021. Comparative Isotherm Analysis of REE Adsorption on Clay-Based Nanocomposites. *Adv. Mater. Res.*, 89(2), 150–160.

Yang, J.; Wang, H., and Zhao, T., 2021. Adsorption Performance of Nanocomposites for REE Recovery at Varying S/L Ratios. *Adv. Mater. Res.*, 89(2), 150–160.

Yang, S.; Huang, X., and Zhang, M., 2021. Acid Leaching and Nanocomposite Adsorption Techniques for Rare Earth Recovery from Industrial Wastes. *J. Hazard. Mater.*, 406, 124671.

Yang, S.; Huang, X., and Zhang, M., 2021. Thermal Behavior and Structural Analysis of Functionalized Nano Clay-Based Adsorbents for Rare Earth Recovery. *J. Hazard. Mater.*, 406, 124671.

Zhang, Y., and Zhao, H., 2017. Clay-Based Nanocomposites: Preparation, Properties, and Applications. *J. Mater. Sci. Eng.*, 2(3), 56–65.

Zhao, Z., and Peng, L., 2014. Synthesis and Application of Nanoclay Composites in Extraction Processes. *Appl. Clay Sci.*, 99, 34–42.

Zhou, X.; Liu, S., and Zhang, H., 2007. FTIR Study on the Interaction Between Montmorillonite and Organic Compounds. *Appl. Clay Sci.*, 36(4), 350–356.